# Integration of Diffusion-Weighted Imaging / Diffusion Tensor Imaging into Radiation Therapy Treatment Planning of Brain Tumors

**Tong Zhu, Ph.D.[1]; Maurice Chojecki, MS[2]; Yue Cao, Ph.D.[3]**

[1] Department of Radiation Therapy, University of North Carolina at Chapel Hill, Chapel Hill, NC, USA
[2] Departments of Radiation Therapy, and Biomedical Engineering, University of Michigan at Ann Arbor, Ann Arbor, MI, USA
[3] Departments of Radiation Therapy, Radiology, and Biomedical Engineering, University of Michigan at Ann Arbor, Ann Arbor, MI, USA

## Introduction

Radiation therapy (RT) is an important part of the standard care for most solid tumor types. The principle of modern RT is to precisely, accurately, and comfortably deliver high energy photon, electron, or heavy charged particle beams to a target volume that consists of solid tumors and high-risk microscopic invasions, while minimizing dose to nearby critical normal tissue structures.

Radiation therapy relies on modern medical imaging techniques to achieve precise target definition and dose delivery verification. Advanced MRI techniques, such as diffusion-weighted and diffusion tensor imaging (DWI and DTI), create unprecedented opportunities to quantify, both spatially and temporally, pathological changes in tumor and normal brain tissue in response to RT. The quantitative measures from the diffusion MRI modalities provide a means for a paradigm-shift in radiation treatment strategy as simultaneously and dynamically assessing tumor response and normal tissue toxicity in the brain.

Here, we present two of our new approaches to integrate quantitative measures from DWI/DTI into treatment planning of radiation therapy for brain tumors.

## High b-value DWI for better target definition of glioblastoma

Accelerated proliferation of tumor cells is identified as one of the three main mechanisms causing failures of radiation therapy [1]. The two most fundamental hallmarks of cancer

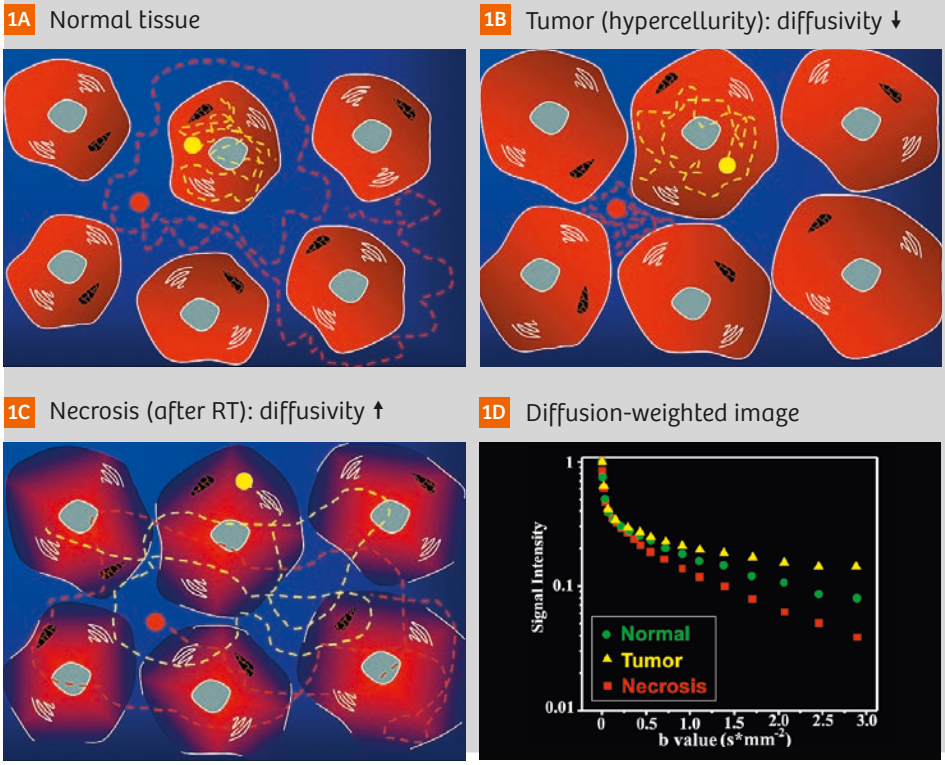


**Figure 1:** Illustration of diffusion MRI for radiation therapy, in terms of **(1B)** tumor detection, **(1C)** evaluation of tumor response to radiation therapy, and **(1D)** potentially increased sensitivity and specificity to normal appearing, non-contrast-enhanced parts of solid tumor using high b-value DWI. *Courtsey and modified from Dr. Yaniv Assaf, Tel Aviv University*

cell are its capability of deregulating the growth-promotion signals and suppress the anti-proliferation signals [2]. Using these mechanisms, cancer cells can maintain a chronic cell proliferation. Consequently, a cascade of aberrant events downstream happens, including accelerated synthesis of DNA, high demand for amino acids that are building blocks of protein and cell membranes, and ultimately high cell density as the results of this aberrant growth of cancer cells.

Diffusion is very sensitive to cell density, intra- and extra-cellular volumes, which can be used for detection of hypercellurity in tumors due to aberrant proliferation. For most solid brain tumors, water diffusion is approximately isotropic. In body temperature, free water diffusion *in vivo* is about 3 x $10^{-6}$ $mm^2$/ms. With a typical b-value of 1000 s/$mm^2$, clinical DWI will measure the displacement of free water molecules of 30 microns. As illustrated in Figure 1, in an image voxel of normal brain white matter tissues (Fig. 1A), intra- and extra-cellular diffusion (represented by yellow and red dots respectively) do not exchange due to the myelin sheath and both contribute to measured diffusion in DWI. In tumoral tissue, cells are highly packed with slightly increased cell size (Fig. 1B). Hypercellularity reduces extracellular diffusion dramatically and increases intracellular diffusion mildly. It leads to an overall decrease in diffusion. Radiation may damage/destroy intracellular organelles, increase cell membrane permeability, and even produce necrosis, which results in a reduction in restricted diffusion between extracellular and intracellular space (Fig. 1C), and an overall diffusion increase. Using a high b-value, fast diffusion signals will attenuate more rapidly than slow ones, the latter is largely from tumor cells due to hypercelluarity and restricted diffusion (Fig. 1D).

In a recent study [3], we explored this unique characteristic of DWI with a high b-value toward detecting enhanced and non-enhanced hypercellular subvolumes of glioblastomas (GB). Glioblastoma is a highly aggressive tumor, and has high intra-tumoral heterogeneity. The standard of care for glioblastoma is resection followed by concurrent and adjuvant chemoRT with temozolomide (TMZ). Standard imaging for RT target definition includes Gd-enhanced T1-weighted and fluid attenuated inversion recovery (FLAIR) T2-weighted MRI. However, tumor heterogeneity and influence of edema and post-surgical inflammation lead to overestimation of the tumor volume by FLAIR images. DWI images with a b-value of 1000 s/$mm^2$ are heavily investigated in clinical research for target definition, tumor grading, and treatment assessment. However, inconsistent ADC values are often reported due to a mixture of high cellular tumor cells, edema, normal tissues, and scar tissues.

We hypothesized that *increasing b-value would improve sensitivity of DWI in detection of tumor with low diffusion due to high tumor cell densities (Figs. 1B, D) and therefore, would potentially improve the accuracy of the gross target volume definition of glioblastoma for radiation therapy.* This study applied DWIs of high b-value up to 3000 s/$mm^2$ to 21 patients with glioblastoma post-resection but prior to chemoradiation. The gross target volume definition for radiation (GTV-Gd) still followed the conventional definition based on post-operative contrast-enhanced T1. Hypercellurity volume (HCV) was first determined on DWIs with a b-value = 3000 s/$mm^2$ within the FLAIR abnormality by using a threshold (the mean intensity plus 2 standard deviations) calculated from a volume of interest in the normal-appearing tissue most contralateral to the tumor. Furthermore, the HCV was divided into Gd-enhanced and non-enhanced components (Figs. 2A, B). Among 15 patients with post-treatment progression, 14 patients had incomplete dose coverage for the pre-treatment HCV (examples from one patient were shown on Figures 2B, C). Patients who had recurrence more rapidly had, on average, a greater percentage of recurrent GTV-Gd spatially overlapping with the pre-RT HCV than those whose recurrence came later. HCV, non-enhanced HCV and the sub-volume of HCV that was not covered by the prescription dose were all significant negative prognostic indicators for the progression free survival ($P < 0.002$, $P < 0.01$ and $P < 0.05$ respectively).

Our results suggested that, in glioblastoma, contrast-T1 imaging underestimates the gross target volume due to missing non-enhanced components and FLAIR overestimates the target volume due to edema and surgery associated inflammation. High b-value DWI could increase the sensitivity and specificity for detection of hypercellular components in glioblastoma and improve accuracy of target delineation. Due to simplicity, high b-value diffusion-weighted imaging likely makes an immediate clinical impact on radiation treatment of brain glioblastoma.

In this study, DWIs in three orthogonal directions with b-values of 1000, 2000, and 3000 s/$mm^2$ were acquired with a 3T MAGNETOM Skyra scanner (Siemens Healthcare, Erlangen, Germany), using the standard single-shot spin-echo echo-planar imaging sequence (ss-EPI). High b-value DWIs were used for assistance of the target delineation. Therefore, imaging parameters of the EPI sequence were carefully selected to balance between achievable geometric accuracy and sufficient signal-to-noise (SNR) level. A GRAPPA = 4 (parallel imaging factor) was chosen to reduce geometric distortion intrinsic to the EPI sequence. We then chose a voxel size with a mean spatial resolution = 1.3 x 1.3 x 5.2 $mm^3$ (range: [1.2–1.4], [1.2–1.4], 5.2 mm) and a mean TE/TR = 99.3/8222 ms (range: 98–105/7400–9200 ms) to obtain a reasonable SNR. Average was also used for high b-value images as 4, 3, and 2 for b = 3000, 2000, and 1000, respectively. Image acquisition for high b-value DWI in this study was quick, typically 2 to 3 minutes, and can be readily implemented in most clinical MRI scanners.

A new diffusion pulse sequence, the read-out segmentation of long variable echo trains technique (RESOLVE), further benefit the needs of radiation therapy. Compared with traditional ss-EPI, RESOLVE [4] effectively shortens echo-spacing with read-out segmentation EPI acquisitions, which leads to reductions in susceptibility and T2* artifact caused geometric distortion, blurring and signal loss. In RESOLVE-EPI, each segment readout is accompanied with

a 2D navigator. RESOLVE not only applies 2D navigators to correct the nonlinear phase variations among segmented readouts but also relies on them as quality indicators to reacquire uncorrectable data, such as signal void from pulsations of the corticospinal fluid (CSF) during the specific segment readout acquisition corresponding to that navigator. Combined with parallel imaging techniques, RESOLVE-EPI will generate high resolution DWIs with improved geometric accuracy, which can potentially improve detectability of small lesions for RT of brain tumors. Our recent experience with the RESOLVE-EPI indicates that the geometric distortion in the brain (except the first 1–2 mm from the brain surface) is unmeasurable compared to the fast spin echo based T1-weighted images.

## Evaluation of radiation-induced white matter injury using an atlas-based, automated DTI tractograph analysis

Quality life for the long-term survivors with benign and low-grade brain tumors and treated by intracranial radiation therapy is important. However, RT, including partial brain RT, has been shown to cause neurocognitive dysfunction [5–10] and affects quality of life of a substantial percentage of long-term survivors. Radiobiologic studies [6–8] have shown that radiation-induced death of neurons is minimal following clinically relevant dose. However, cognitive function is carried out by neural networks, supported by white matter (WM) pathways, rather than single cortical structures (i.e. the hippocampus). DTI combined with fiber tracking techniques allows us to assess individual fiber bundle response to radiation dose and contribution to changes in cognitive functions after RT.

The decline in executive function is one of the most common patterns of cognitive declines observed in patients with benign and low-grade cranial tumors after RT. The executive function is mainly carried out in the neural network consisting of the prefrontal functional cortical regions, such as dorsal lateral prefrontal cortex (DLPFC), and the WM fiber bundles including the inferior fronto-occipital fasciculus (IFOF). However, the common decline in executive function seems to be contradictory to the heterogeneous tumor locations of the patients, where the high doses were delivered (Fig. 3). When the network involved in the executive function is considered, it is not a surprise.

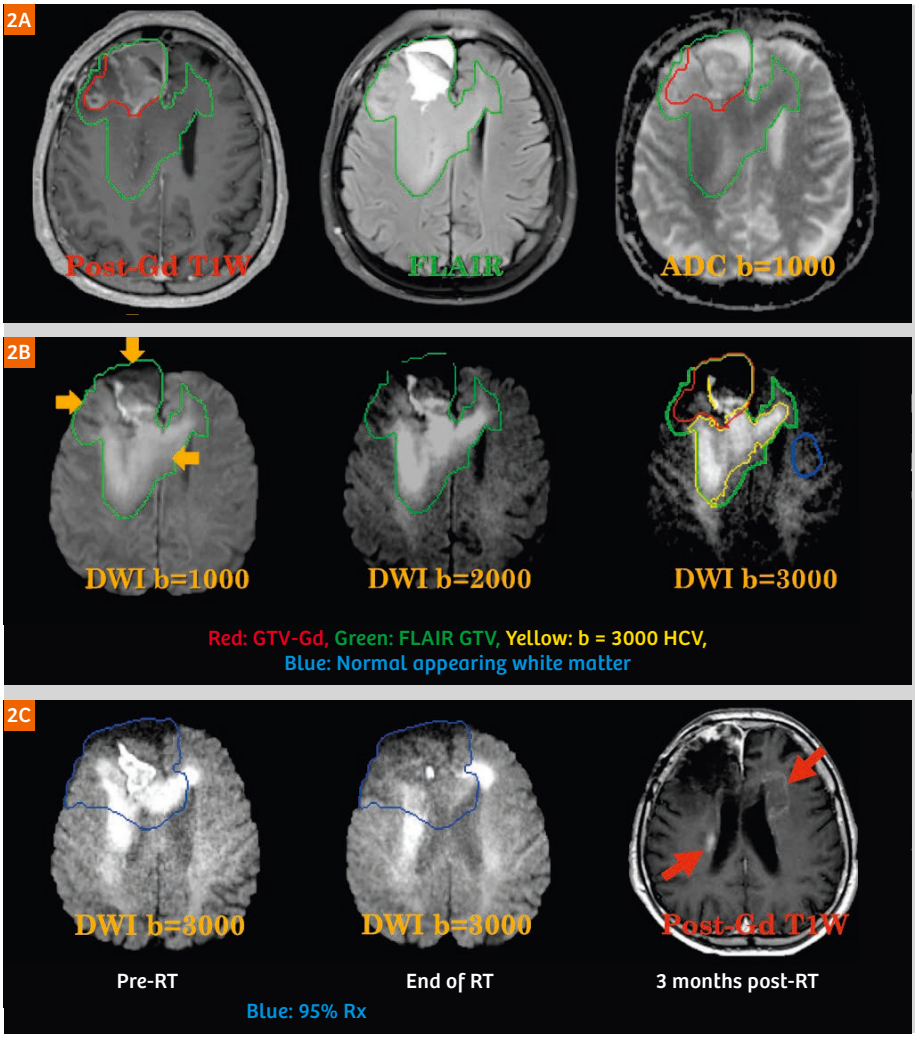


**Figure 2:** High b-value DWI for detection of hyper-cellularity in patients with non-contrast enhanced sub-volume of glioblastoma. **(2A)** There was no difference in depicting tumor volume between post-Gd T1 (red contour, also used as the gross target volume for RT) and conventional ADC maps acquired with a b-value of 1000 s/mm$^2$. FLAIR images overestimated the tumor volume (green contour) due to edema. **(2B)** With a b-value of 3000 s/mm$^2$, it attenuated fast water diffusion such as those from edema and normal tissues. Contributions from slow water diffusion from high density tumor cells were enhanced (yellow contours). **(2C)** Compared to high b-value DWI images pre-RT (left column), hyper-cellular tumor tissues within volumes defined by the 95% prescription isodose line from the treatment plan for the GTV defined by the pre-treatment Gd-enhanced T1 MRI (middle column) were largely killed by radiation treatment. However, Gd-enhanced T1 of the recurrent tumors (red arrows in the right column) clearly showed large overlapping between recurrence and the sub-volumes of pre-treatment HCV that were not covered by radiation.

In a recent study [11], we hypothesized that *subject-specific radiation damage to different sections of the same WM network could result in a similar neurocognitive outcome, and WM bundles could respond to a maximum radiation dose, much like a serial structure.* To test the hypothesis, we conducted a longitudinal DTI study of 33 patients with low-grade or benign cranial tumors underwent partial brain RT. MRI scans were performed at six time points: 1–2 weeks pre-RT, 3 and 6 weeks during RT, and 1, 6, and 18 months after RT. We implemented an atlas-based, automated DTI WM tractograph analysis to segment 22 major WM bundles of the whole brain of 33 patients from DTI data of six time points to relate longitudinal WM changes to radiation dose and specific neurocognitive outcomes. Our study found that long inter-cortical association and projection WM bundles responded to the maximum dose received by the bundles, like a typical serial structure. This type of dose response cannot be discovered without DTI and fiber tracking. Also, we found that axial diffusivity (AD) decreased progressively over time, and 20 Gy (EQD2) caused significant changes in DTI-derived measures.

3

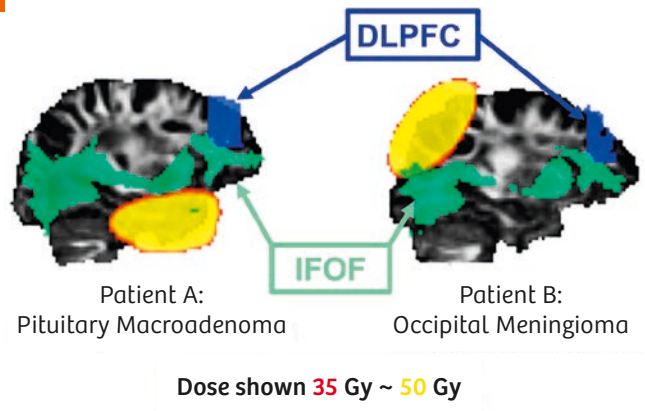


**Figure 3:** Typical examples of heterogeneity of primary tumor locations / high dose regions vs. common patterns of neurocognitive decline post-RT among patients with low-grade/benign cranial tumors. Both patients experienced decline in executive and long-term memory functions related to the dorsolateral prefrontal cortex (DLPFC). Both patients had high-dose regions (dose larger than 35 Gy are shown in the map with orange to bright yellow colors) distal to the DLPFC but overlapped at different sections of the inferior fronto-occipital fasciculus (IFOF), an essential part of the DLPFC neural network.

4

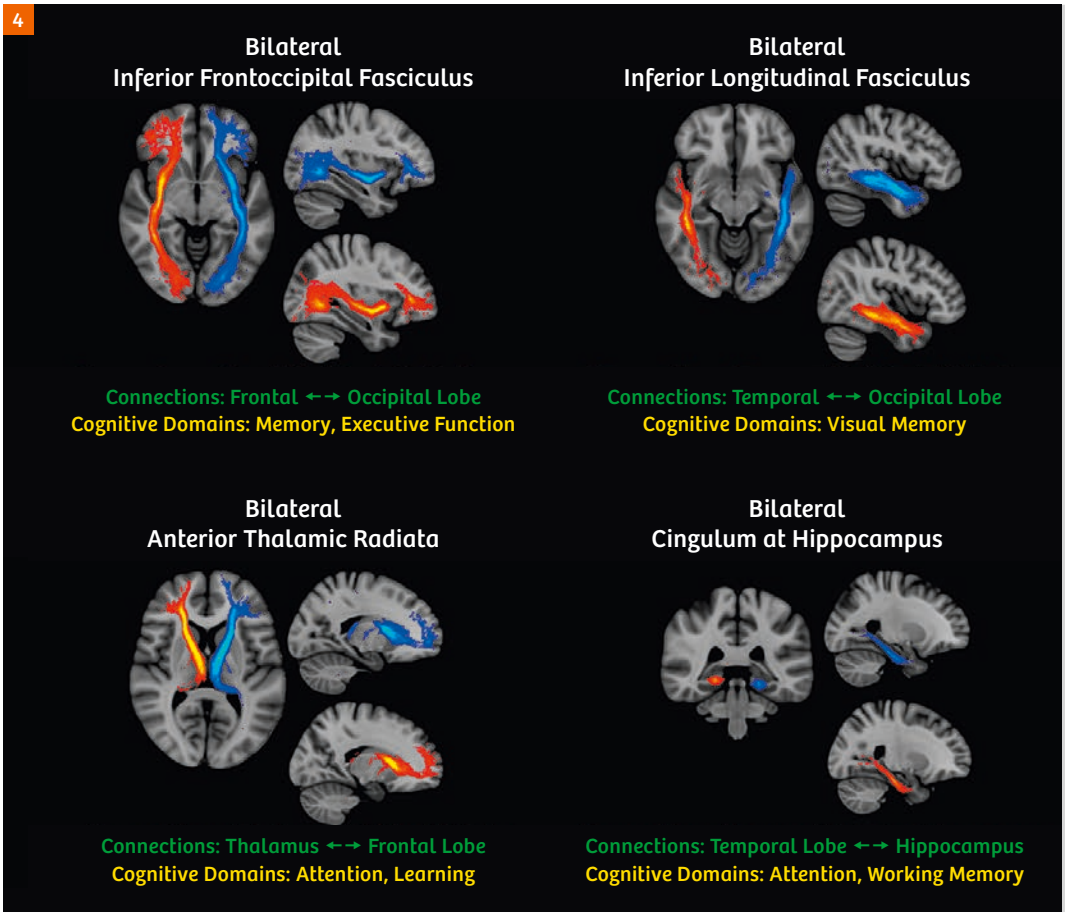


**Figure 4:** Examples of long inter-cortical association and projection WM fiber bundles where longitudinal changes in WM following RT significantly correlate with the maximal dose received by the bundles, with their anatomical inter-cortical connections and their known involvements in cognitive domain labelled.

The dose response patterns observed in our study could provide a new insight on how to plan radiation doses in the long-term survivors to reserve critical cognitive functions. In current clinical practice, the guidelines [12] are only limited to spare brain stem and optic nerves/chiasm. Sparing critical white matter fibers to reserve cognitive functions is achievable by the state-of-art radiation therapy techniques, such as intensity modulated radiation therapy / volumetric modulated arc therapy (IMRT/VMAT). Several fiber bundles that show the significant dose effects in our study are known to be essential parts of neural networks for executive functions, working memory and decision making (Fig. 4). To test the feasibility of reducing the maximum dose to less than 20 Gy for key WM bundles without compromising the planned target volume (PTV) coverage, we further carried out a preliminary study of nine patients who experienced decline in executive functions post-RT. Nine WM bundles were identified with major to minor roles in the network of executive functions, including the genu of the corpus callosum (Callosum), bilateral arcuate fasciculi (Arcuate), bilateral inferior fronto-occipital fasciculi (IFOF), bilateral superior longitudinal fasciculi (SLF), as well as bilateral uncinate fasciculi (Uncinate). VMAT plans were generated, and the V20 (i.e. the percentage of volume in WM bundles receiving dose at least 20 Gy) for each bundle was calculated for plans optimized with and without WM sparing. Our results showed that PTV doses were the same with and without WM sparing. The 5 patients who had pituitary or nasal tumors, or tumors located in the anterior temporal lobe had 77% or greater of WM bundles spared with the V20 less than 5%. For the 4 patients with tumors located in the frontal lobe or the mid brain, it was impossible to spare the ipsilateral WM bundles and the genu of corpus callosum, however sparing 22–30% of contralateral WM bundles such as the accurate fasciculus and the SLF was achieved. DVHs from treatment plans with and without WM sparing of one patient are shown in Figure 5 as examples.

A whole-brain DTI scan can be done in 3–5 minutes. An example protocol of DTI that we used on a 3T MAGNETOM Skyra scanner is as following: TR = 4600 ms and a minimized TE, resolution = 1.72 x 1.72 x 3.9 $mm^3$, b-value = 1000 $s/mm^2$, a GRAPPA factor of 2, the number of unique diffusion-weighting directions = 20, two repeat measurements and a total scan time of 3 minutes and 40 seconds for coverage of a whole brain. To quantify the robustness of automated tractograph analysis on clinically acquired DTI data, we used the Jaccard Similarity Index (JSI) to evaluate the within-patient similarity of pairs of tracked and binarized fiber bundles at any two time points, and achieved a mean JSI of 0.85 over all WM bundles from all patients scanned on the Siemens scanner, equivalent to 90% of volume overlap of the same bundle tracked longitudinally. This indicated high repeatability of our method and also excellent DTI quality for conducting robust DTI tractrograph analyses.

## Discussion

Quantitative measures from DWI and DTI have been successfully applied to radiation therapy of brain tumors for evaluation of tumor response [13] and for understanding radiation-induced brain injury on selected white matter structures [14, 15]. Recent developments in MRI, especially

5

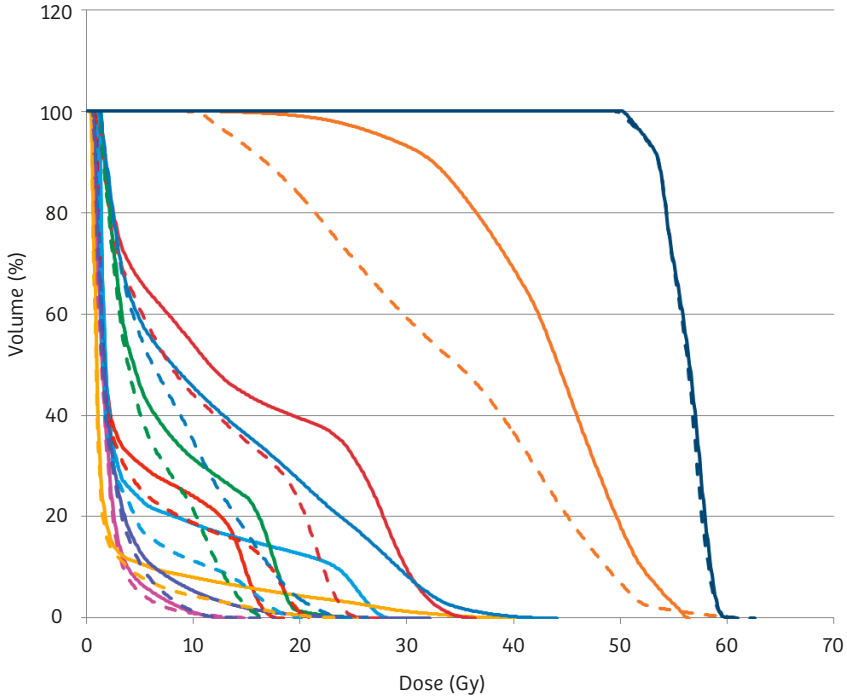


**Figure 5:** DVHs of WM bundles with (dashed lines) and without (solid lines) WM sparing.

parallel imaging [16–18] and parallel RF transmission [19] that improve imaging acquisition efficiency and reduce image artifacts due to geometric distortion, enable us to acquire high-quality DWI images with high b-value and high-quality DTI within a clinically feasible time frame to explore two new clinical applications of

1) improving detectability of non-enhanced hypercellular subvolumes of glioblastoma for radiation therapy and,
2) better understanding of radiation dose response of WM fiber pathways within the whole brain using robust and efficient DTI tractograph analyses respectively.

Our study of high b-value DWI for glioblastoma raises an exciting hypothesis that boosting the hypercellular volume delineated by high b-value DWI could delay time to progression, which is an area for future study. The new information that elongated association and projection fiber bundles respond like a serial structure, could provide a new insight into radiation treatment planning to preserve critical cognitive functions in long-term survivors. A preliminary treatment planning study also demonstrated the feasibility of dose sparing of critical WM fiber pathways without compromising the prescribed dose to the planned target volume.

While clinical applications of DWI/DTI in radiation therapy of brain tumors are promising, several limitations of DWI/DTI have impacts on their applications in radiation therapy, for example, the trade-off among overall image quality, acquisition time and geometric accuracy. Geometric distortions from susceptibility and eddy current artifacts, which are intrinsic to EPI sequences, may lead to increased uncertainty in target definition. Imaging acquisition of DWI/DTI with segmented EPI techniques like the RESOLVE-EPI DWI/DTI [4], fast spin-echo based imaging sequences such as fast spin echo PROPELLER DWI [20], and variable density spiral DTI sequence [21] could potentially improve geometric accuracy and achievable image resolution. There are still a lot of works need to be done to optimize MRI sequences, protocols and workflow for radiation oncology applications. Finally, robust QA procedure should be implemented and evaluated periodically in order to reduce variation in ADC measurement due to system performance.

**References**

1 Joiner M, van der Kogel A. Basic clinical radiobiology 4th edition. Hodder Arnold, London, 2009.
2 Hanahan D, Weiberg RA. Hallmarks of cancer: the next generation. Cell 2011; 144:646-674.
3 Pramanik PP, Parmar HA, Mammoser AG, Junck LR, Kim MM, Tsien CI, Lawrence TS, Cao Y. Hypercellularity Components of Glioblastoma Identified by High b-Value Diffusion-Weighted Imaging. Int J Radiat Oncol Biol Phys 2015; 92:811-819.
4 Porter DA, Heidemann RM. High Resolution Diffusion-Weighted Imaging Using Readout-Segmented Echo-Planar Imaging, Parallel Imaging and a Two-Dimensional Navigator-Based Reacquisition. Magn Reson Med 2009; 62:468-475.
5 Sheline G. Radiation therapy of brain tumors. Cancer 1977; 39:873-881.
6 Tofilon PJ, Fike JR. The radioresponse of the central nervous system: A dynamic process. Radiat Res 2000; 153:357-380.
7 Soussain C, Ricard D, Fike JR, et al. CNS complications of radiotherapy and chemotherapy. Lancet 2009; 374:1639-151.
8 Greens-Schloesser D, Robbins ME, Peiffer AM, et al. Radiation-induced brain injury: a review. Front Oncol 2012; 2:73. doi: 10.3389/fonc.2012.00073.
9 Klein M, Heimans JJ, Aaronson NK, et al. Effect of radiotherapy and other treatment-related factors in mid-term to long-term cognitive sequelae in low-grade gliomas: a comparative study. Lancet 2002; 360: 1361-1368.
10 Douw L, Klein M, Fagel SSA, et al. Cognitive and radiological effects of radiotherapy in patients with low-grade glioma: long-term follow-up. Lancet Neurol 2009; 8: 810-818.
11 Zhu T, Chapman C, Tsien C, Spratt D, Lawrence T, Cao Y. Effect of the maximum dose on white matter fiber bundles utilizing longitudinal diffusion tensor imaging. Int J Radiat Oncol Biol Phys 2016; 96:696-705.
12 Marks LB, Yorke, ED, Jackson A, Ten Haken RK, Constine LS, Eisbruch A, Bentzen SM, Nam J, Deasy JO. Use of Normal Tissue Complication Probability Models in the Clinic. Int J Radiat Oncol Biol Phys 2010; 76:S10-S19.
13 Galban CJ, Hoff BA, Chenevert TL, Ross BD. Diffusion MRI in early cancer therapeutic response assessment. NMR Biomed 2016; doi: 10.1002/nbm.3458
14 Nagesh V, Tsien CI, Chenevert TL, et al. Radiation-induced changes in normal-appearing white matter in patients with cerebral tumors: A diffusion tensor imaging study. Int J Radiat Oncol Biol Phys 2008; 70:1002-1010.
15 Chapman CH, Nagesh V, Sundgren PC, et al. Diffusion tensor imaging of normal-appearing white matter as biomarker for radiation-induced late delayed cognitive decline. Int J Radiat Oncol Biol Phys 2012; 82:2033-2040.
16 Sodickson DK, Manning WJ. Simultaneous acquisition of spatial harmonics: fast imaging with radiofrequency coil arrays. Magn Reson Med 1997; 38:591–603
17 Pruessmann KP, Weiger M, Scheidegger MB, Boesiger P. SENSE: sensitivity encoding for fast MRI. Magn Reson Med 1999; 42:952–962.
18 Griswold MA, Jakob PM, Heidemann RM, et al. Generalized autocalibrating partially parallel acquisitions (GRAPPA). Magn Reson Med 2002; 47:1202–1210.
19 Katscher U, Börnert P. Parallel RF transmission in MRI. NMR Biomed. 2006; 19:393-400.
20 Pipe JG, Farthing VG, Forbes KP. Multishot diffusion-weighted FSE using PROPELLER MRI. Magn Reson Med. 2002; 47:42-52.
21 Frank LR et al., High Efficiency, Low Distortion 3D Diffusion Tensor Imaging with Variable Density Spiral Fast Spin Echoes (3D DW VDS RARE). Neuroimage 2010; 49: 1510-1523.

**Contact**

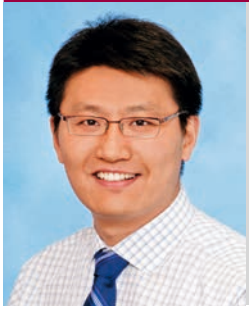

Assistant Professor Tong Zhu, Ph.D.

Department of Radiation Therapy
University of North Carolina at Chapel Hill

CB# 7512, NC Cancer Hospital
101 Manning Dr
Chapel Hill, NC 27599-7512
USA
tong_zhu@med.unc.edu